# Physics-based Modelling and Simulation of Reverberating Reflections in Ultrasonic Guided Wave Inspections Applied to Welded Rail Tracks

Dineo A. Ramatlo[1*], Craig S. Long[2], Philip W. Loveday[3] and Daniel N. Wilke[1]

[1] *Department of Mechanical and Aeronautical Engineering, University of Pretoria, Pretoria, 0002, South Africa*

[2] *Manufacturing Cluster, Council for Scientific and Industrial Research, Pretoria, 0001, South Africa*

[3] *School of Mechanical, Industrial and Aeronautical Engineering, University of the Witwatersrand, Johannesburg, 2000, South Africa*

[*] *dineo.ramatlo@up.ac.za*

**Abstract**

The development of ultrasonic guided wave monitoring systems has become increasingly important as they have demonstrated the ability to detect damage in structures. An example of such a system is the Ultrasonic Broken Rail Detection system which uses pitch-catch piezoelectric transducers permanently attached to the rail to excite and receive ultrasonic guided wave signals. Changes in signals can provide a reliable indication of damage growth in the rail and ultimately reduce broken rails and derailments. However, the challenge during system development is obtaining monitoring data containing damage signatures as damaged sections of rail are immediately replaced when detected. Laboratory damage experiments are also not plausible due to end reflections from short rail sections dominating the response. Modelling and simulation thus become increasingly important to enable the simulation of unavailable damage scenarios for the upgradation of existing (or development of new reliable) guided wave-based monitoring systems.

Two numerical procedures to model and simulate guided wave inspections encompassing the excitation, propagation and scattering from discontinuities in 1D waveguides are presented and applied to the inspection of the web of a welded rail. The major contribution highlighted by these procedures is the ability to simulate complex back and forth reverberating reflections. These reflections occur between various reflectors such as welds and other discontinuities such as damage. The two methods are different but complementary. The first one, which is based on a simple manual simulation of finite reverberating reflections, is useful for interpreting the results to understand how different reflections interact, especially where they overlap. The second method accounts for the scattering by all defects or discontinuities arbitrarily positioned in the waveguide. It offers a more accurate approximation of the simulated inspection since it accounts for infinite reflections.

The simulation results obtained from the two modelling procedures are validated using a field experiment from a damage-free rail containing welds and holes as discontinuities. The results show that it would be possible to simulate inspections for unavailable damage scenarios. The paper is concluded with a thorough analysis of the inspection measurement using the first method.

*Keywords:* Welded rail inspection; Guided wave ultrasound; Modelling and simulation; Direct reflections; Reverberating reflections

## 1. Introduction

Permanently installed Guided Wave Ultrasound (GWU) based inspection systems have demonstrated the ability to provide a solution to currently intractable inspection problems [1, 2]. These systems deploy sensors at a fixed position in a pitch-catch or pulse-echo manner and collate the GWU signals over time. An example of such a system is the guided wave-based Ultrasonic Broken Rail Detection (UBRD) system which can interrogate or monitor large volumes of a railway line (up to hundreds of meters) from a single transducer location [3, 4, 5].

GWU systems are susceptible to discontinuities and can be designed to distinguish benign structural features from defects, using knowledge of how wave propagation modes interact with various geometrical features. Changes in signals can provide a reliable indication of damage growth and, ultimately, a reduced false alarm rate. The earliest detection of accumulating damage would allow more time to take action and avoid broken rails and derailments. Recent research shows that underlying damage signatures can be detected using the conventional

baseline subtraction method and widely used computational techniques such as singular value decomposition and independent component analysis (ICA) [6, 7, 8]. Liu et al. [8] demonstrated that component methods perform significantly better than the residual method, with ICA generally producing the best defect detection. Loveday et al. [5] recently applied the two component methods to operational data from a heavy haul line. They demonstrated that it is possible to detect and locate a transverse defect in the head of the rail. The artificial defect in this field experiment was introduced by glueing a small mass under the head of the rail at a distance of 370m from an array of two transducers.

Monitoring of rail track may involve the propagation of ultrasonic guided waves over several hundred metres or thousands of wavelengths and is complicated in operational railway lines. In addition to dispersion, attenuation and scattering of the waves from discontinuities in the rail, the guided wave propagation is also affected by the amount of rail grinding that had been performed, the foundation of the ballast, the sleepers, rail clips, and electrical cables attached to the rail. The complex interaction of guided waves with changing environmental and operation conditions (EOCs) is evident in measurements performed on an operational rail track. EOC changes introduce signal variations limiting the size of the defect that can be detected. Temperature is the most common cause of signal variation, [9, 10], and as it is a physics-based property, we could model it by varying the Young's Modulus of the rail. It affects the propagation velocity of the guided waves, leading to the varying arrival times of the reflections from discontinuities. Moreover, these EOCs such as temperature may vary along the length of the rail and with time.

The authors in [8] demonstrated a procedure based on temperature compensation and receiver operating characteristic (ROC) to quantify system performance under real operational conditions. The disadvantage of this scheme is that the generation of the ROC requires different scenarios of monitoring data containing complex reflections from benign structural features and growing damage under varying environmental conditions. This is often impractical but can be achieved by fusing experimental data collected from an undamaged structure exposed to different EOCs with synthetic damage signatures, as demonstrated by Liu et al. [8] with an application in pipelines. Recent advancements in research on temperature compensation methods can be found in references [11, 12, 13, 14]. The idea in references [11, 12] is to stretch the signals by some factor to compensate for wave velocity changes induced by varying temperatures. In addition to velocity changes, the authors in [13] also address the phase changes often caused by the frequency response of the transduction system and present an improved procedure in [14]. This compensates for other temperature dependant effects caused by attenuation and relative amplitudes of different modes excited by the transducer.

In railway lines, other identified EOCs which introduce time-varying coherent noise into measured data include effects of passing trains and rail track sinking into the ballast. The foundation of the ballast could vary at different locations in the rail, and the welds, which are present in the field, are not all identical. Setshedi et al. [15] recently showed that it is possible to account for wear by estimating rail properties that best fit experimental measurements. Other effects, however, are more complex and difficult to compensate for. Multiple propagating modes which are dispersive over long-range propagation further complicate the nature of the signals making it almost impossible to identify damage signatures. Furthermore, obtaining monitoring data for different damage scenarios under varying EOCs is virtually impossible for railway lines since detected defects in sections of an operational rail track are immediately removed and replaced with new rail. Laboratory damage experiments are also not possible due to end reflections from short sections of rail dominating the response. Modelling and simulation thus become increasingly important to better understand the complex nature of GWU and ultimately enable the upgradation of existing (or development of new reliable) GWU-based monitoring systems. Finally, modelling is also necessary to simulate the very complex scattering of propagating modes from discontinuities. More importantly, features that are not apparent in the experiment, such as unavailable damage scenarios. For the case of railway lines, we need numerical models to simulate damage signatures.

A complete guided wave inspection involving excitation, propagation and scattering of guided waves can be modelled and simulated using the traditional 3D Finite Element Method (FEM) with an explicit time domain solver [16, 17, 18]. However, the drawback is that only relatively short sections of the waveguide can be considered. Long et al. [19] demonstrated that the challenge of end reflections in explicit solvers could be eliminated by adding absorbing regions at the two ends of the 3D waveguide to simulate an infinitely long waveguide. However, the simulation results were computed at a distance of 1m from the excitation point, and the entire 3D domain was less than 5m in length. This 3D FEM problem was solved for a rail waveguide without any

discontinuities, and it was the largest that the author could solve at that time. In this paper, we consider over hundreds and hundreds of meters of inspection range, which would be impractical to solve due to high computational demands. Various numerical modelling approaches for GWU have been proposed in the literature, though many focus on separate aspects of an inspection. The Semi-Analytical Finite Element (SAFE) method is the widely used approach for modelling wave propagation in 1D waveguides as it allows for long-range propagation. However, it requires that the cross-section of the waveguide remains constant. The method employs a 2D cross-section of the waveguide discretised using semi-analytical finite elements and applies analytical variations along the length of the waveguide to predict the waves at a specific location [20, 21]. SAFE can also predict and analyse the dispersion and attenuation of propagating modes required to develop signal processing strategies [21, 22, 23].

Recently, hybrid approaches combing SAFE and 3D FEM have been developed to study the scattering of guided waves from complex discontinuities and their excitation using piezoelectric transducers, respectively. Benmeddour et al. [24] introduced a hybrid method addressing the former, which uses a 3D FEM model of an arbitrary discontinuity and two SAFE models to represent the semi-infinite incoming and outgoing waveguides. This method was used to predict reflection amplitudes from discontinuities in rails such as aluminothermic welds and defects such as cracks [25, 26], indicating that it should be possible to detect defects in rails at long-range before complete breaks occur [26]. A second hybrid approach addressing the latter was developed by Loveday [27]. The method couples a 3D FEM model of a piezoelectric transducer with a 2D SAFE model of the elastic waveguide and accounts for transducer dynamics. The method has been refined and verified in [19, 28]. The same authors demonstrated how the technique could be employed to design and optimise resonant piezoelectric transducers to preferentially excite desired modes in rails [28], offering insights into how the location and dynamics of a transducer influence the excitation of guided wave modes.

To date, only a few authors have reported the implementation of numerical models to simulate a complete guided wave-based inspection. However, most of these models involve exciting the guided waves from one end of the waveguide and reflecting either from the free-end or a single discontinuous feature. This makes them inappropriate for long continuous waveguides such as pipelines and rails, where inspections are usually carried out in both directions, and many discontinuities are present. The authors in [16, 17, 18] excited the guided waves by simply employing nodal forces. Jezzine et al. [29] mounted a simple transducer model accounting only for normal stresses at the end of a semi-finite 1D waveguide and computed the guided wave reflections from a normal crack. Later they developed a method to compute scattering from more general structural features and defects with complex geometry [30, 31]. This method has been integrated into the analysis software called CIVA [32]. Baronian et al. [33] demonstrated the application of the CIVA software to simulate the scattering of guided waves caused by several discontinuities in a waveguide by introducing the notion of a scattering matrix. The scattering matrix provides a link between the incoming and outgoing guided waves between discontinuities and generalises the discontinuities as a single scattering domain. Although the method was successfully applied for short-range propagation (less than tens of metres) where a relatively short time signal was required, the approach could be adopted for long-range propagation (over hundreds of metres), but the effects of attenuation and dispersion in the time domain would need to be accounted for.

Ramatlo et al. [34] presented a physics-based modelling approach to simulate a realistic ultrasonic guided wave-based inspection of a waveguide with multiple discontinuities using piezoelectric transducers. The paper demonstrated how relevant modelling aspects involving excitation with a transducer [27, 19, 28], propagation over long distances [20, 21] and scattering from complex features [24, 25, 26], which were separately considered in the previous literature could be consolidated into a single modelling framework. The effects of transducer dynamics, attenuation and dispersion, which are prominent due to the significant inspection range, were accounted for. Attenuation in the rail was approximated by determining the optimal hysteretic and viscous damping parameters using a model updating procedure as explained in [34]. The modelling framework was validated against a field measurement in the head of a rail and demonstrated that it is possible to carry out an inspection from a single transducer location while accounting for reflections from multiple discontinuities on the two sides of the source, though it considers only direct reflections from welds.

In addition to direct reflections that occur when a guided wave is reflected only once from each discontinuity, there are other complex reflections where a guided wave reflects multiple times from two or more discontinuities until all the energy has been attenuated. The phenomenon of reverberating reflections is also common in other

fields where researchers model and simulate the propagation of waves in multilayer structures. For example, the propagation of seismic waves in multiple layers of the earth [35], ray propagation modelling to characterize different types of materials [36], wave propagation in multi-segment transmission lines [37] and non-destructive evaluation of adhesively bonded structures [38]. In GWU, researchers in [39] applied an advanced signal processing method in guided wave testing for pipelines to minimize background noise and enhance the signal quality. Their results showed that it is possible to identify small damage reflections and repeat echoes caused by the scattering from welds and damage. Although this phenomenon is not significant when the guided waves are excited in the head of a rail, it becomes evident when the waves are excited in the web region and should be accounted for as the excited mode reflects strongly from welds [25, 26]. Fig. 1 shows a schematic representation of a series of direct reflections (plotted in black arrows), where the guided waves reflect (R) off a single weld. An example of a multiple reflection between two welds is shown using red arrows. The excited guided waves propagate forward to weld A, reflect (R) from A and propagate backward, transmit (T) through the transducer and propagate to weld B where the second reflection happens, causing the waves to propagate forward again. This multiple reflection is called a double reflection. Examples of head and web measurements from an operational rail showing direct and multiple reflections from the welds are shown in Fig. 2.

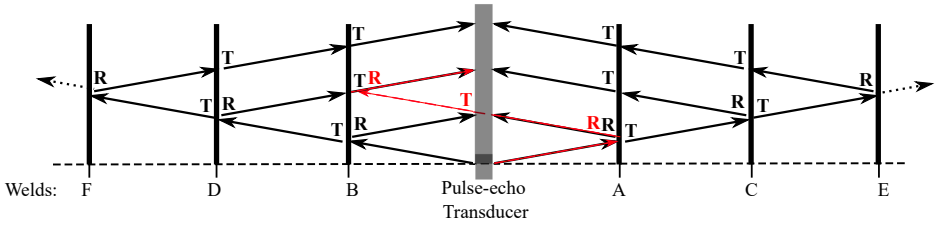


Fig. 1. Representation of direct reflections (in black) and a double reflection between two welds (in red). R (Reflection) and T (Transmission).

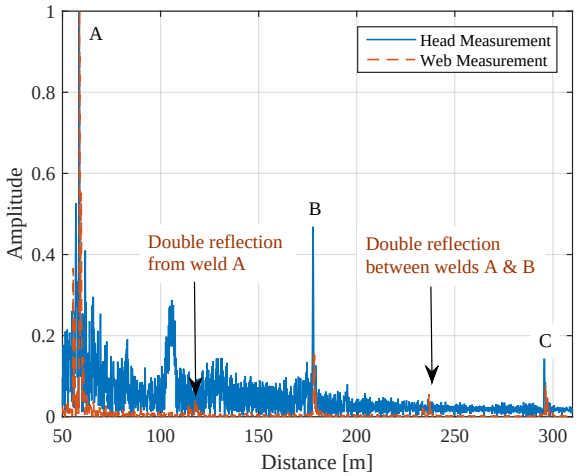


Fig. 2. Examples of head and web measurements from a rail showing normalised direct reflections from welds A, B and C as well as double reflections in the web measurement.

The modelling framework in [34] can be adopted to simulate reverberating reflections in a complete configuration of GWU-based inspection by simulating each reflection path separately and calculating the resultant response. However, if many multiple reflections are to be included in the simulation, the process would be tedious and cumbersome since each combination of reflections would have to be simulated manually by carefully following a path traced by the waves propagating the multi-discontinuous waveguide. The method could thus

be adapted to simulate only a finite number of reflections that are not too complex. However, suppose this modelling framework is integrated with the method of Baronian et al. [33] for generalising the propagation and scattering between several discontinuities. In this case, it will be possible to account for all multiple reflections occurring in a waveguide section.

This paper aims to demonstrate physics-based approaches to model and simulate a complete guided wave inspection in long-range monitoring. We consider an operational rail with welds and holes in the web as discontinuities and attempt to capture the complex network of reverberating reflections caused by these multiple discontinuities. We employ models of excitation by a piezoelectric transducer, propagation of guided waves and scattering from welds (and other present discontinuities) as presented in [34] to first perform the simulation considering a finite number of reflections. Second, the relevant computation principles from [34] are then integrated with the method of Baronian et al. [33] as follows: (i) compute a global scattering matrix for a series of discontinuities on the right-hand side of the transducer, (ii) compute a global scattering matrix for a series of discontinuities on the left-hand side of the transducer, (iii) couple the global scattering matrices for the right and left waveguides with the hybrid models of excitation by a transducer and scattering from a transducer to simulate and compute the received guided wave reflections. Although the two approaches are based on the same models of individual elements in the rail, they are different but complementary. The first one is based on simple manual simulation of finite reverberating reflections and offers the ability to perform a thorough analysis of the resultant simulation to better understand how different reflections interact with each other, especially where they overlap. The second method is based on a general scattering matrix computation and offers a more accurate approximation of the simulated inspection since it accounts for infinite reverberations. The complementary capabilities of the two approaches that offer the advantage of interpretable results and better reconstruction makes them very attractive when used together. This paper intends to highlight this feature. The two modelling approaches will be useful when developing a digital twin model of the rail, as outlined in reference [34].

The complexities discussed earlier are difficult to model and are thus not accounted for in the two physics-based approaches employed in the paper. The authors are not aiming to capture the complex variations caused by EOCs as a lot of factors cannot be quantified. Perfect agreement between the field experiment and simulation results is therefore not expected. The objectives of this paper are (1) to capture the correct propagating mode excited by the transducer, and reflection distances as well as dispersion and attenuation in the rail, (2) to account for multiple reflections in the inspection and (3) to explore the complementary nature of the two modelling approaches. In the third objective, we investigate the advantages and disadvantages of each approach and further investigate the benefit of using them together. We highlight that, given some state of a model, either a low or high fidelity model, the principles of reverberating reflections that we learn will remain unchanged. While the second approach gives a better reconstruction, the first approach will always allow the researcher to interpret as much as they can.

The novelty of the paper is summarized as follows:

- We present a new approach to simulate the complex network of reverberating reflections caused by multiple discontinuities. Although our infinite reflections model is based on the method in reference [33], the authors did not demonstrate this feature in their paper. The method presented in [33] was only applied to a semi-infinite waveguide, where the transducer was attached to the end of this waveguide. This method is extended, in our paper, to the case of an infinite waveguide extending in both directions from the transducer.
- We demonstrate the benefit of using two modelling approaches to complement each other. The paper does not consider simulation and modelling from a generative point of view only like most researchers do in the literature, but also looks at them from an interpretable point of view. The first approach helps to interpret the results, while the second approach helps to get a better approximation of the inspection measurement.
- We highlight the phenomenon of multiple reflections in a rail waveguide and simulate reflections propagating over hundreds of meters from the excitation point. The phenomenon of multiple reflections in railway lines has not been presented before in the literature. Although some results from pipelines indicated this, the inspection was in the range of tens of meters and therefore less complex.

Section 2 describes a guided wave-based inspection of the web section of an operational rail track and presents the situation to be modelled, and provides the experimental result. The modelling and simulation

of the inspection following the framework in [34] is described in Section 3.1, and Section 3.2 presents the integration of modelling elements from this framework with the method of Baronian [33] to simulate infinite multiple reflections in multi-discontinuous waveguides. The simulation results are presented in Section 4 and validated using the experimental measurement. A thorough analysis of the GWU inspection is presented in Section 4.3, where the modelling and simulation framework in [34] is employed to simulate finite multiple paths and interpret the GWU inspection. The conclusions are finally drawn in Section 5.

## 2. GWU inspection in the web of a rail

A GWU-based inspection was performed on an operational heavy haul line with 240m long sections of UIC60 rail joined together in the field by aluminothermic welding. The weld cap produced was ground off the top and sides of the railhead but remained around the remainder of the circumference of the rail. The rail also contained two holes going through the longitudinal section in the web. These changes in the cross-section of the rail cause reflections of guided waves at the welds and holes. A piezoelectric transducer was attached to the web of the rail at a distance of approximately 59m from the nearest weld. The first hole (hole B) was located approximately 1m before the transducer and the second one (hole A) approximately 3m before weld A. Fig. 3 shows the rail setup. The transducer was driven by a 17.5 cycle Hanning windowed tone burst voltage source with a centre frequency of 35kHz, as shown in Fig. 4. The voltage applied to the piezoelectric element induced vibrations in the transducer, which induced a guided wave field in the rail.

The transducer transmits guided waves in both directions along the rail. After excitation, the transducer was used to receive signals corresponding to the energy reflected from welds and holes located on either side of the transducer. The measurement obtained from the field experiment, which will be simulated in this paper, is plotted in Fig. 5. The signal clearly shows the reflections from the welds and holes, with an exponential loss of energy from the hole closest to the transducer (hole B) to the furthest weld (weld E), whose reflection is masked by the coherent noise.

A short time Fourier Transform was applied to the measured time domain signal to produce a time-frequency spectrogram, as shown in Fig. 6. The mode-shape of the most dominant mode in the measurement is plotted in Fig. 7. This mode was identified by comparing arrival times of different frequencies with estimates based on the distances to the welds/holes and the group velocity predictions for different modes from a SAFE model of the rail. The predicted arrival time as a function of frequency for a web mode (Fig. 7) was then plotted as a curve on the spectrogram for identified reflections. If this curve coincided with a domain of higher energy in the spectrogram, then it was concluded that this reflection was captured in the measurement. This signal contains only one significant mode of propagation which is simpler than the case of multiple modes propagating in the head of the rail considered in [34]. However, this signal is complicated by the presence of multiple reflections.

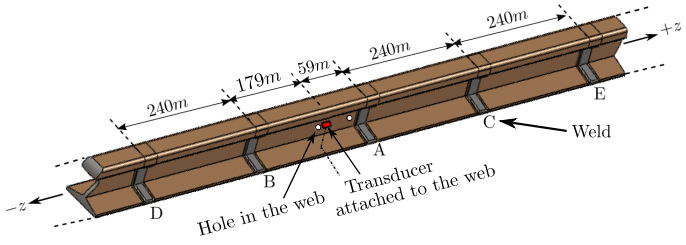


Fig. 3. Configuration of the waveguide for web measurement.

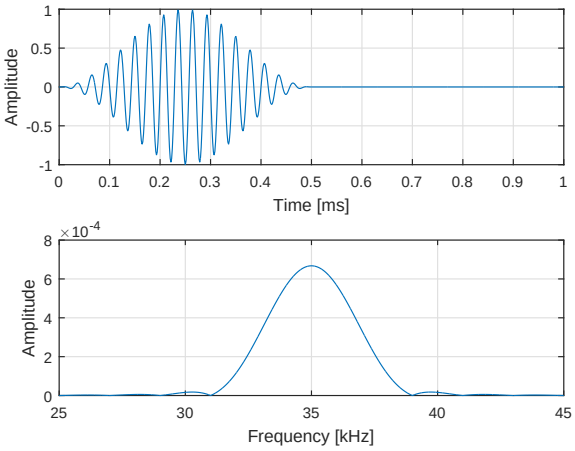


Fig. 4. Excitation signal in time and frequency domains.

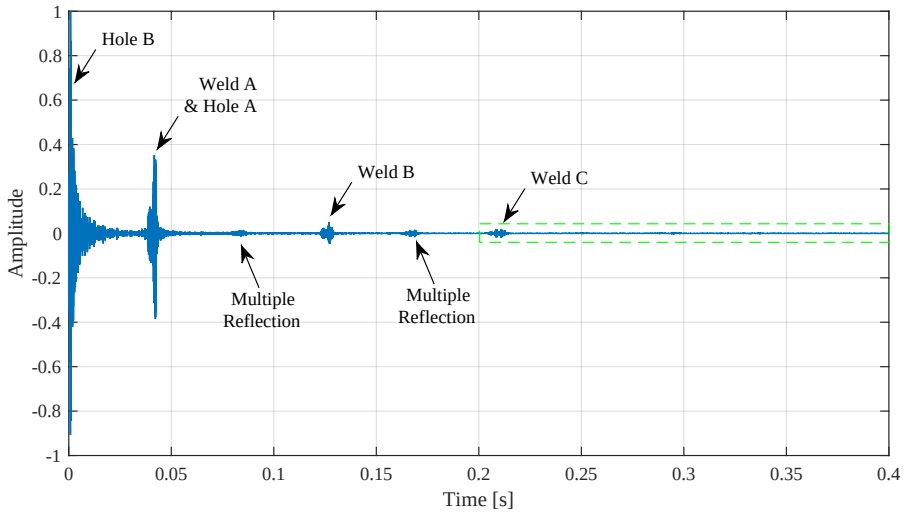


(a)

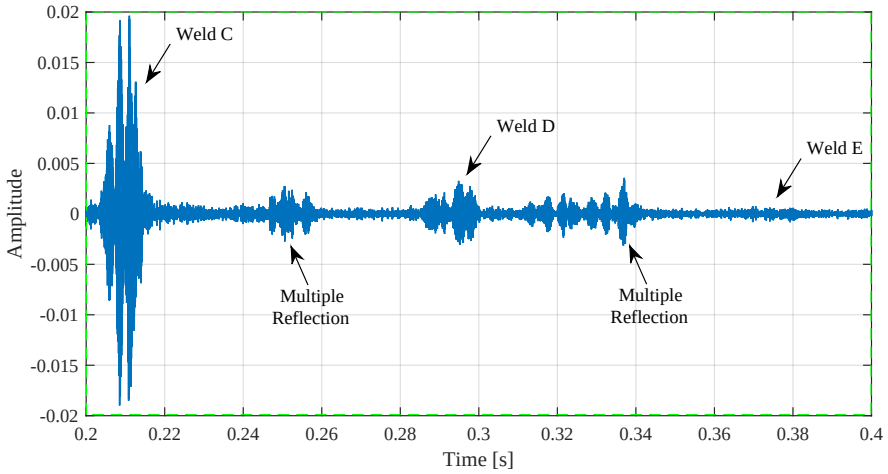


(b)

Fig. 5. The measurement obtained from the field experiment. (a) Direct reflections from welds and holes and multiple reflections. (b) Reflections from welds C to E and other multiple reflections.

The field measurement presented in this section will be modelled and simulated in the next section.

## 3. Modelling and simulation of a guided wave inspection

This section presents different modelling elements that form the basis of the two approaches and illustrates how the modelling elements are consolidated together in each approach to model and simulate multiple reflections in waveguides with multiple discontinuities. Sections 3.1 and 3.2 explain the two approaches for modelling finite multiple reflections and infinite multiple reflections, respectively.

The first step in the modelling and simulation of a complete guided wave inspection involves modelling individual elements of the inspection, which usually comprises four main parts: the excitation, propagation, scattering and reception of guided waves. In this paper, we adopt and couple together three separate numerical

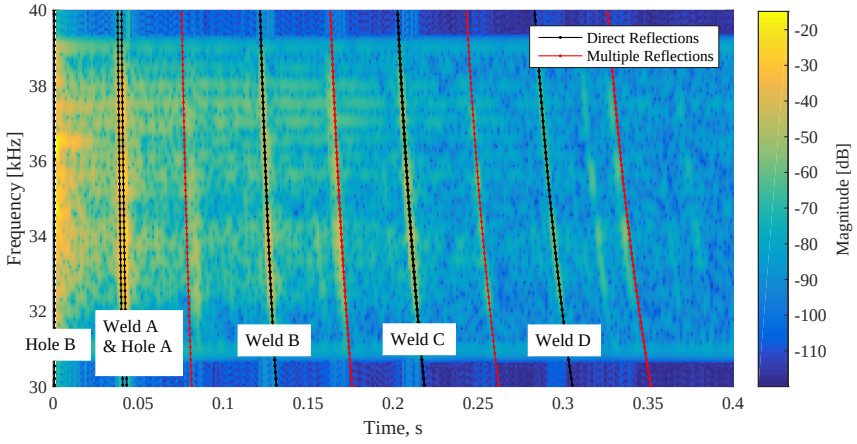


Fig. 6. A spectrogram of the field measurement showing the arrival times of the direct and multiple reflections for the web mode.

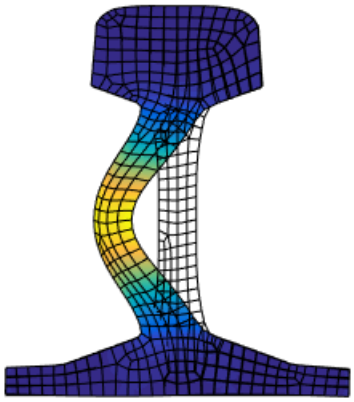

Fig. 7. The mode shape with energy concentrated in the web section, at 35kHz.

models for the first three parts and achieve the latter by a simple computation of a displacement response of a node on the waveguide. Fig. 8a shows the numerical models of the different elements of the inspection and examples of results achieved from each model.

For the inspection setup in Fig. 3, we first consider guided wave propagation in regions of constant cross-sectional areas in the rail. The regions of constant cross-sectional area are modelled using a SAFE method presented in [20], which discretizes the displacement field across the cross-section of the waveguide using 2D finite elements. The propagation of guided waves along the waveguide length is achieved by applying analytical variations in the $z-$direction. The SAFE method solves for the wavenumbers and corresponding mode shapes supported by the waveguide. These wave properties are solved at selected frequency points and used to compute other dispersion properties of the waveguide, such as the phase and group velocities. The attenuation in the rail was modelled using damping, and the damping coefficients were determined using the optimisation procedure explained in [34].

The excitation of guided waves in the rail using a piezoelectric transducer was modelled using a hybrid model which couples a 3D FEM model of a transducer and a 2D SAFE model of the waveguide. This hybrid model is explained in detail in references [27, 19, 28, 40]. The model properly accounts for transducer dynamics, which is important when resonant transducers are employed, such as in this case. The hybrid method for GW excitation solves for the modal amplitudes of the propagating modes, given a voltage applied to the piezoelectric transducer. The hybrid model for guided wave excitation is shown in Fig. 8a. The piezoelectric transducer is attached to the web of the rail. It is designed to preferentially excite a mode with energy concentrated in the web section (depicted in Fig. 7). This mode is known to propagate long distances and reflects strongly from welds [25, 26]. Fig. 8a also shows the modal amplitudes computed for a unit voltage at each frequency point.

The scattering of guided waves from reflectors is modelled using a second hybrid model, which couples a 3D FEM model of the reflector with two SAFE models to represent the semi-infinite incoming and outgoing rails on either side of the reflector. For the system considered in this paper (Figs. 3 and 8a), the reflectors in the rail are the welds and holes in the web section. The hybrid model for guided wave scattering solves for the modal amplitudes of the reflected and transmitted guided waves for each incident mode by enforcing continuity and equilibrium on the boundaries of the left and right semi-infinite waveguides intersecting the 3D volume of the reflector. The results are presented in reflection and transmission coefficient matrices, respectively, as shown in Fig. 8a. The hybrid method for modelling guided wave scattering from reflectors is explained in detail in the paper by Benmeddour [24].

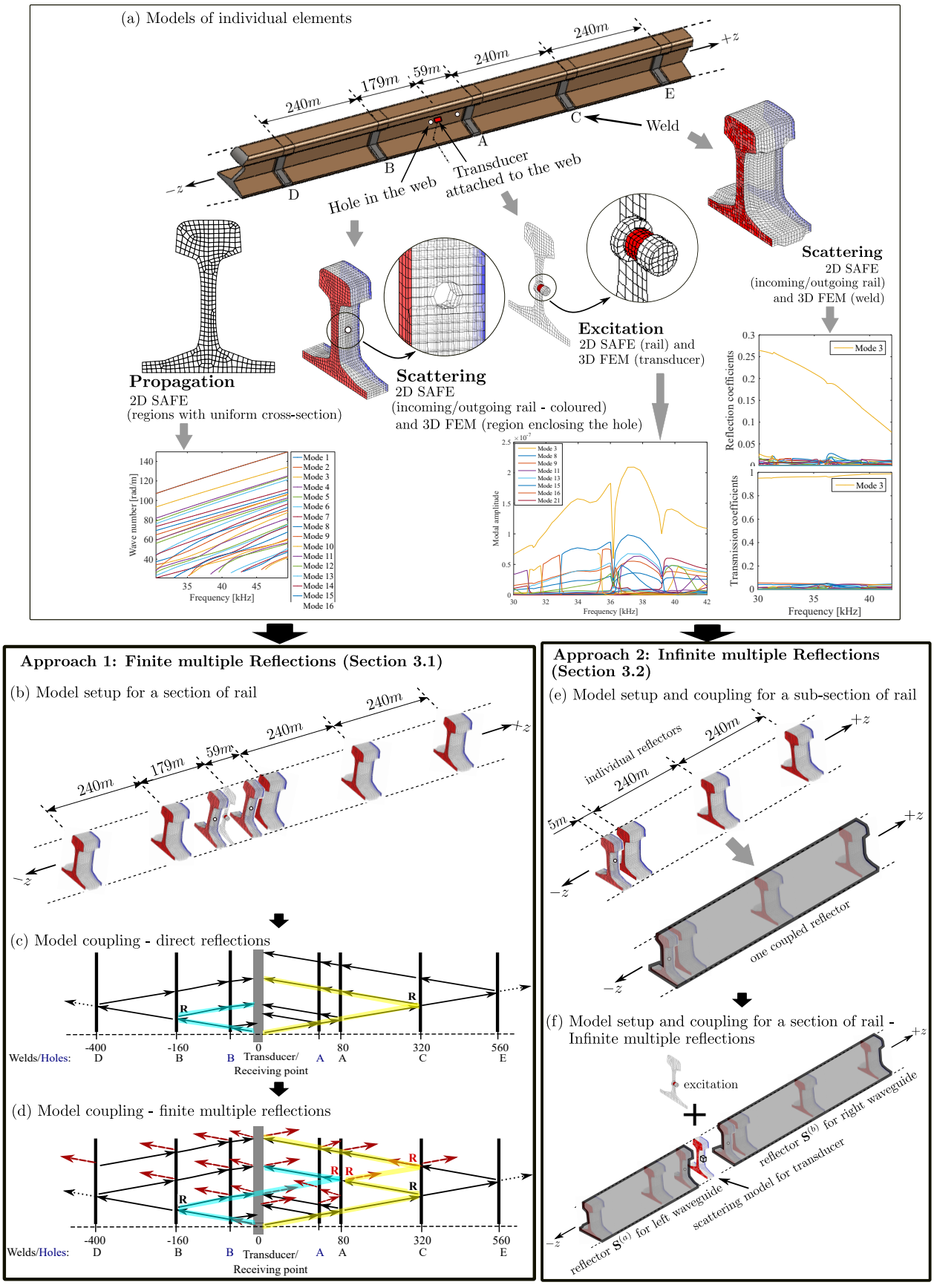


Fig. 8. Modelling and simulation of a GWU inspection using the two approaches.

The hybrid models of the welds and holes were solved only once, respectively, since it was assumed that all the welds and holes have the same geometry. Another hybrid model not depicted in Fig. 8a but later adopted in the two simulation procedures is that of the scattering from the transducer. All the models were solved at a selected range of frequencies and assuming a constant excitation. The results were stored in a database. The model data was later interpolated according to the excitation signal in Fig. 4, and adopted in the two approaches used in this paper to simulate the finite and infinite multiple reflections of the propagating waves, respectively.

### *3.1. Finite multiple reflections*

Figs. 8b-d illustrate the modelling and simulation of finite multiple reflections using the modelling framework in [34]. The models of individual elements from Fig. 8a are adopted and set up as illustrated in Fig. 8b to represent a model of the section of rail considered. The model contains one hybrid model of the rail and transducer for guided wave excitation, five hybrid models to represent welds A to E and two more hybrid models to represent the two holes in the web of the rail. The first hole is located on the right side of the transducer (just before weld A), and the second hole is located on the left side of the transducer. Fig. 8c shows a schematic representation of how direct reflections from welds and holes in the rail are computed using the modelling framework in [34]. A direct reflection means that the guided waves excited by the transducer are propagated to a specific reflector (while being transmitted through the preceding reflectors), reflected from that reflector and propagated backwards in the opposite direction (while being transmitted through the preceding reflectors) back to the transducer location. Examples of two direct reflections, one from weld B and the other from weld C, are highlighted in Fig. 8c.

Fig. 8d illustrates how the method in [34] is extended to include the simulation of multiple reflections between the reflectors in the rail. A multiple reflection means that the guided waves would reverberate between the reflectors before propagating back to the transducer location. Examples of two multiple reflections are highlighted in Fig. 8d. Other multiple reflections can be achieved by propagating the waves according to the black and red arrows and computing the response at the reception point by tracing the path followed by the waves. It is thus possible to efficiently add or remove paths since this is a post-processing step and requires several transmission and reflection matrix multiplications, as explained in [34]. This approach is the first adopted to simulate finite multiple reflections.

### *3.2. Infinite multiple reflections*

The second approach adopted in this paper employs the modelling elements in [34] and [33] to simulate infinite multiple reflections in the inspection. This method also employs the models of individual elements from Fig. 8a and aims to represent several local reflectors as one reflector by introducing a single scattering matrix. Fig. 8e illustrates this method where the four reflector models (one hole and three welds) on the right-waveguide (to the right of the transducer) are coupled together to create a single domain of reflectors for the considered sub-section of rail. The application of this modelling procedure is illustrated in Fig. 8f. The general scattering matrix for this region is computed using the reflection and transmission matrices for each reflector. The computation accounts for the complex reverberations of guided waves between the reflectors and attenuation. The method is adopted to create a model for the entire section of rail considered in the complete inspection. The method of Baronian et al. is first used to couple the reflectors on the left and right waveguides, respectively. After that, these reflectors are coupled with a scattering model of the transducer.

Consider a sub-section of rail indicated by the right waveguide from the configuration presented in Fig. 8. This section has four reflectors, namely hole A and welds A, C and E, with associated reflection and transmission matrices as indicated and explained in Section 3 and Fig. 8a. The four reflectors are coupled together to represent a single domain with a general scattering matrix $\mathbf{S}$ of reflection and transmission coefficients by applying the procedure in [33] as illustrated in Fig. 8e. The same procedure is applied in this section, as illustrated in Fig. 8f, to demonstrate the modelling of a complete inspection. Fig. 9 shows a simple representation of the model similar to Fig. 8f for a section of rail.

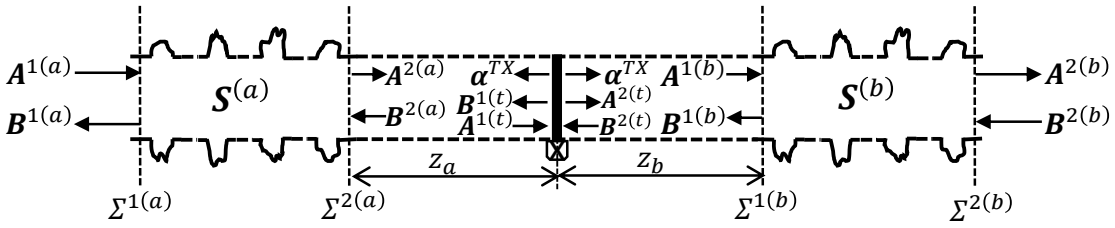


Fig. 9. Model setup and coupling for simulation of infinite multiple reflections.

The hybrid model for guided wave excitation using a piezoelectric transducer is represented by the modal amplitudes of the excited guided waves denoted as $\alpha^{TX}$ in Fig. 9. These waves will propagate in the two opposite directions from the transducer location. On the left and right of the transducer are two sub-sections of hybrid rail models. Each is made of two semi-infinite waveguides and a 3D domain of several reflectors in between, bounded by surfaces $\sum^{1(*)}$ and $\sum^{2(*)}$ for each domain $*$ represented by $a$ and $b$, respectively.

Outside the domain $*$ of reflectors, the wave fields are expressed using modal expansions by splitting modal coefficients into right-going components ($\mathbf{A}^{1(*)}$ and $\mathbf{A}^{2(*)}$) and left-going components ($\mathbf{B}^{1(*)}$ and $\mathbf{B}^{2(*)}$), where superscripts 1 and 2 refer to guided wave modes on the boundaries $\sum^{1(*)}$ and $\sum^{2(*)}$, respectively. The magnitudes of incoming modes $\mathbf{\Psi}^{(*)}_{\mathbf{in}} = \left\{\mathbf{A}^{1(*)}, \mathbf{B}^{2(*)}\right\}^T$ and outgoing modes $\mathbf{\Psi}^{(*)}_{\mathbf{out}} = \left\{\mathbf{B}^{1(*)}, \mathbf{A}^{2(*)}\right\}^T$ are related to each other according to the general scattering matrix $\mathbf{S}^{(*)}$ as follows:

$$\mathbf{\Psi}^{(*)}_{\mathbf{out}} = \mathbf{S}^{(*)}\mathbf{\Psi}^{(*)}_{\mathbf{in}} \tag{1}$$

with

$$\mathbf{S}^{(*)} = \begin{bmatrix} \mathbf{R^{1}}^{(*)} & \mathbf{T^{2}}^{(*)} \\ \mathbf{T^{1}}^{(*)} & \mathbf{R^{2}}^{(*)} \end{bmatrix} \tag{2}$$

The scattering matrix $\mathbf{S}^{(*)}$ is composed of four sub-matrices of reflection coefficients ($\mathbf{R^{1}}^{(*)}$, $\mathbf{R^{2}}^{(*)}$) and transmission coefficients ($\mathbf{T^{1}}^{(*)}$, $\mathbf{T^{2}}^{(*)}$) for $N$ finite incident waves incoming on $\sum^{1(*)}$ and $\sum^{2(*)}$, respectively.

Similarly, modal expansion is also applied to the scattering model of the transducer domain $t$:

$$\mathbf{\Psi}^{(\mathrm{t})}_{\mathbf{out}} + \alpha^{TX}\left\{1,1\right\}^T = \mathbf{S}^{(\mathrm{t})}\mathbf{\Psi}^{(\mathrm{t})}_{\mathbf{in}} \tag{3}$$

with

$$\mathbf{S}^{(\mathrm{t})} = \begin{bmatrix} \mathbf{R^{1}}^{(t)} & \mathbf{T^{2}}^{(\mathrm{t})} \\ \mathbf{T^{1}}^{(t)} & \mathbf{R^{2}}^{(t)} \end{bmatrix} \tag{4}$$

The two scattering domains, $a$ and $b$ and the transducer domain, are separated by portions of waveguides of lengths $z_a$ and $z_b$, respectively. A global scattering matrix for the configuration in Fig. 9 is sought.

In the waveguide portion between domain $a$ and the transducer $t$, it is possible to write continuity relations between the magnitudes ($\mathbf{A}^{1(t)}$ and $\mathbf{A}^{2(a)}$) and ($\mathbf{B}^{1(t)}$ and $\mathbf{B}^{2(a)}$) since waves propagate without distortion as guided waves in this region. The continuity relation can be written by employing the propagation matrix denoted as $\mathbf{P}^{(at)}$, which involves modal propagators of the $N$ modes considered in the modal decomposition:

$$\mathbf{A}^{1(t)} = \mathbf{P}^{(at)}\left(\mathbf{A}^{2(a)}\right) \tag{5}$$

$$\mathbf{B}^{1(t)} = \left(\mathbf{P}^{(at)}\right)^{-1}\mathbf{B}^{2(a)} - \alpha^{TX} \tag{6}$$

Continuity between domain $b$ and the transducer relates the magnitudes ($\mathbf{A}^{1(b)}$ and $\mathbf{A}^{2(t)}$) and ($\mathbf{B}^{1(b)}$ and $\mathbf{B}^{2(t)}$) according to the propagation matrix $\mathbf{P}^{(bt)}$:

$$\mathbf{A}^{1(b)} = \mathbf{P}^{(bt)}\left(\mathbf{A}^{2(t)} + \alpha^{TX}\right) \tag{7}$$

$$\mathbf{B}^{1(b)} = \left(\mathbf{P}^{(bt)}\right)^{-1}\left(\mathbf{B}^{2(t)}\right). \tag{8}$$

The propagation matrix is given by:

$$\mathbf{P}^{(*t)} = diag\left(e^{-j\kappa_n z_*}\right)_{1\leq n\leq N} \tag{9}$$

where $\kappa_n$ is the complex wavenumber of the $n^{th}$ mode accounting for attenuation and is computed using SAFE, and $z_*$ is the propagation distance between the transducer and reflector $*$.

The equations in Eq. (1), Eq. (3) and Eqs. (5-7) yield a system of $10-equations$ and $10-unknowns$ which could be solved simultaneously. The incoming components $\mathbf{A}^{1(a)}$ and $\mathbf{B}^{2(b)}$ are incident modes coming from the left and right sides of the considered rail section. In our case, these modes are set to zero as the only source of guided waves is the transducer shown in Fig. 9.

After solving for the modal amplitudes $\mathbf{A}^{1(t)}$ and $\mathbf{B}^{2(t)}$, the frequency response can be calculated:

$$U(z,\omega) = \sum_{n=1}^{N} \mathbf{A}^{1(t)}\psi_n^+ + \sum_{n=1}^{N} \mathbf{B}^{2(t)}\psi_n^- \tag{10}$$

and then converted to the time domain by applying an inverse Fast Fourier transform.

## 4. Results

The simulation results for the rail inspection described in Section 2 are presented here. We first start with the presentation of the simulated inspection containing infinite multiple reflections, where the procedure in Section 3.2, which is based on the paper of Baronian et al. [33] was adopted. The result of the same inspection simulated using the procedure in Section 3.1, where a finite number of reflections were manually included, is presented afterwards. As outlined in the introduction, the intention of this paper is not to capture the complex variations caused by EOCs as many factors cannot be quantified. Perfect agreement between the field experiment and simulation results is therefore not expected. The aim is to capture a complex network of reverberating reflections caused by multiple welds and holes in the web of the rail, and to highlight that, given some state of a model, either a low or high fidelity model, the principles of reverberating reflections that we learn will remain unchanged.

The first objective is to capture the correct propagating mode excited by the transducer, and reflection distances as well as dispersion and attenuation in the rail. This requirement is demonstrated by the results presented in Sections 4.1 and 4.2, which were produced using the two approaches described in Sections 3.2 and 3.1, respectively. The second objective, which is to account for infinite multiple reflections in the inspection, is addressed in Section 4.1, where a good reconstruction of the simulation is obtained from the infinite multiple reflections approach. Although this approach is efficient and yields realistic results, it does not offer an understanding of how these reverberations come about. The results from the finite multiple reflections approach, presented in Section 4.2, addresses this gap by explaining the propagation paths traced by the waves during those reverberations. In Section 4.3, a thorough analysis of the result is carried out to demonstrate further how the finite multiple reflections can be adapted to interpret the complexities of the simulated inspection. The third objective of the paper is to explore the complementary nature of the two modelling approaches and investigate the advantages and disadvantages of each approach. This objective is addressed by the whole of Section 4 by highlighting that, while the infinite multiple reflections approach gives a better reconstruction, the finite multiple reflections approach will always allow the researcher to interpret as much as they can.

### *4.1. Simulation of infinite multiple reflections*

Firstly, the resultant simulated time domain signal computed using all propagating modes and infinite multiple reflections is considered. Figs. 10a&b depicts the envelope of the simulated time domain response, normalised with respect to the maximum amplitude of the first reflection, together with the measured signal normalised in the same way. The reflections from the simulated welds and holes are annotated and clearly visible. Several dominant reflections were identified based on the experience of the inspection setup, and analysis of the field measurement in Section 2 and the results in Figs. 10 and 11. The most notable characteristics, namely the arrival times of the dominant reflections, dispersion, attenuation and the location of multiple reflections, are accurately captured in the simulated result. This result is considered in more detail in Figs. 10c-h, which depicts the details around each reflection. The reflection coming from the hole closest to the transducer, hole B

in Fig. 10c, was badly approximated due to high coherent noise in this region and also because the near-field infinite multiple reflections which are caused by a series of sleepers attached to the foot of the rail around the transducer region were not included in the simulation. These reverberations between several close-by scatterers are visible in the field measurement in Fig. 10c. Moreover, other propagating modes probably exist close to the transducer. Though this region is outside the detection range as explained by Loveday in [5], the effect of infinite reflections, which this paper aims to account for, is visible here. The approximation of the other reflections in Figs. 10d-h appears to be very acceptable. The direct reflections from a set of two reflectors that are very close to each other, weld A and hole A, separated by an approximate distance of about 5m, are shown in Fig. 10d. It is clear that the energies of these direct reflections do not overlap, though each reflection contains an overlap of multiple energies caused by dispersion. Traces of coherent noise from factors such as attenuation and dispersion is evident throughout the signal.

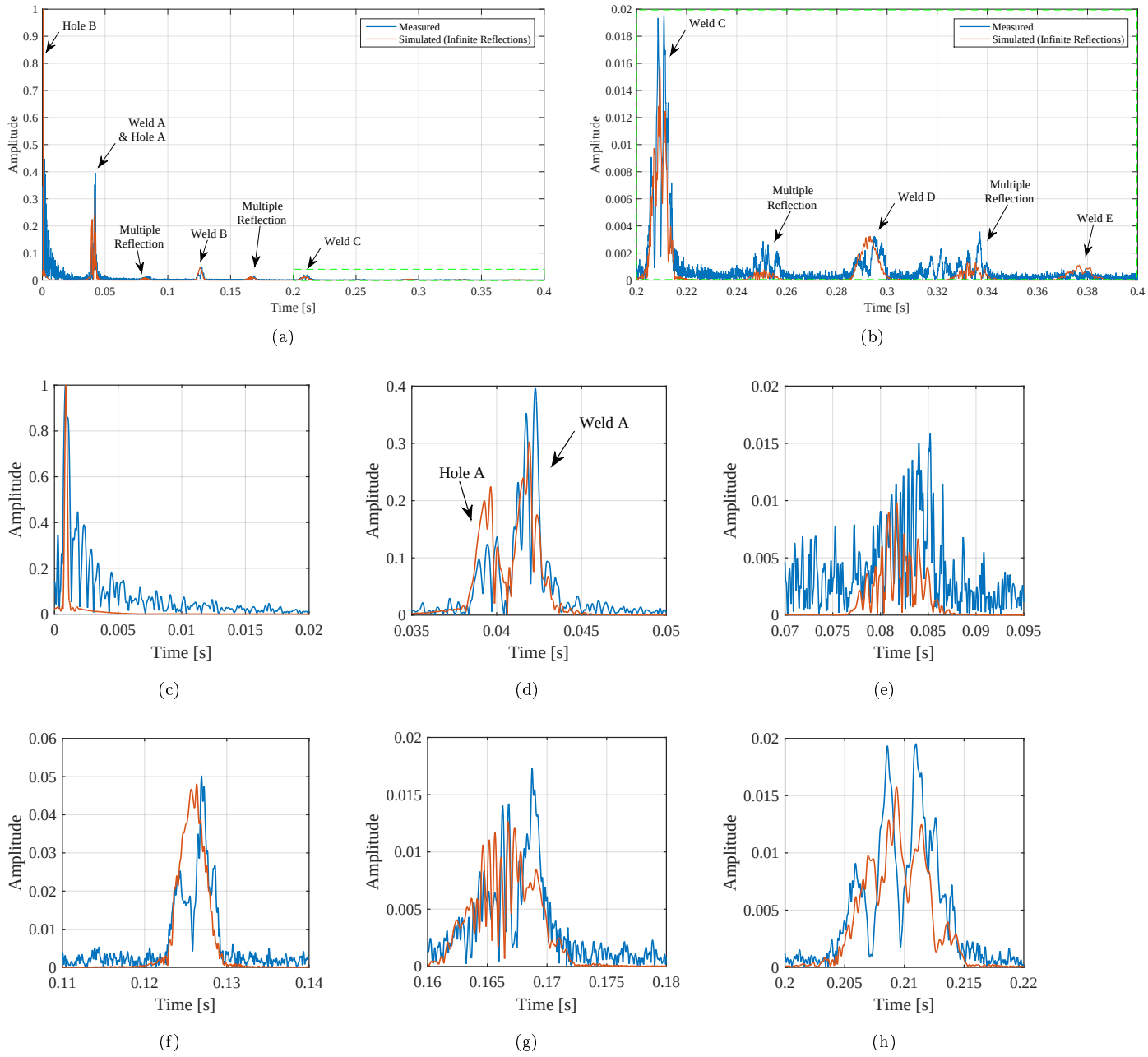


Fig. 10. Time history of the measured and simulated signals containing infinite reflections. Reflections from (a) welds A to C and the two holes, as well as multiple reflections, (b) welds C to D and other multiple reflections, (c) hole B, (d) weld A and hole A. (e) Multiple reflection. (f) Reflections from weld B. (g) Multiple reflection. (h) Reflections from weld C.

The direct reflections from welds B and C have also been well approximated though some details were absent in the simulated signal (Figs. 10f&h). Fig. 10 shows that in general, multiple reflections (Figs. 10e&g) are far more complex than direct reflections, with the identified multiple reflections arriving first in time (at approximately 0.08s) being the most complex as a result of high coherent noise and other variations in this region almost masking this reflection. It is noted that other apparent multiple reflections shown in Fig. 10b, which arrive at approximately 0.25s and 0.33s, were not well approximated. However, the simulated result looked good and was very helpful with the identification of these reflections. There is another reflection arriving at approximately 0.32s in the field measurement, which was not captured by the simulation, and the reason for this is currently unknown. This reflection could have come from a hole and/or cable attached to the web of the rail that was not included in the model. The authors might not have kept records of all holes during the field experiment. If there was indeed a missed reflector that was not modelled, its contribution as well as the sleepers and other factors affecting the field experiment as discussed in the introduction, would also explain the amplitude difference that we see when comparing the field and simulated measurement. The last feature of the simulation worth noting at this point in Fig. 10b, is the reflection from weld E which is clearly visible in the simulated result and mostly masked by noise in the field measurement. This highlights the benefit of modelling and simulation and their potential to enable data-driven approaches such as digital twins. The simulation procedure made it possible to easily spot this reflection that is not apparent in the field measurement and also helped identify the source of each reflection in the inspection.

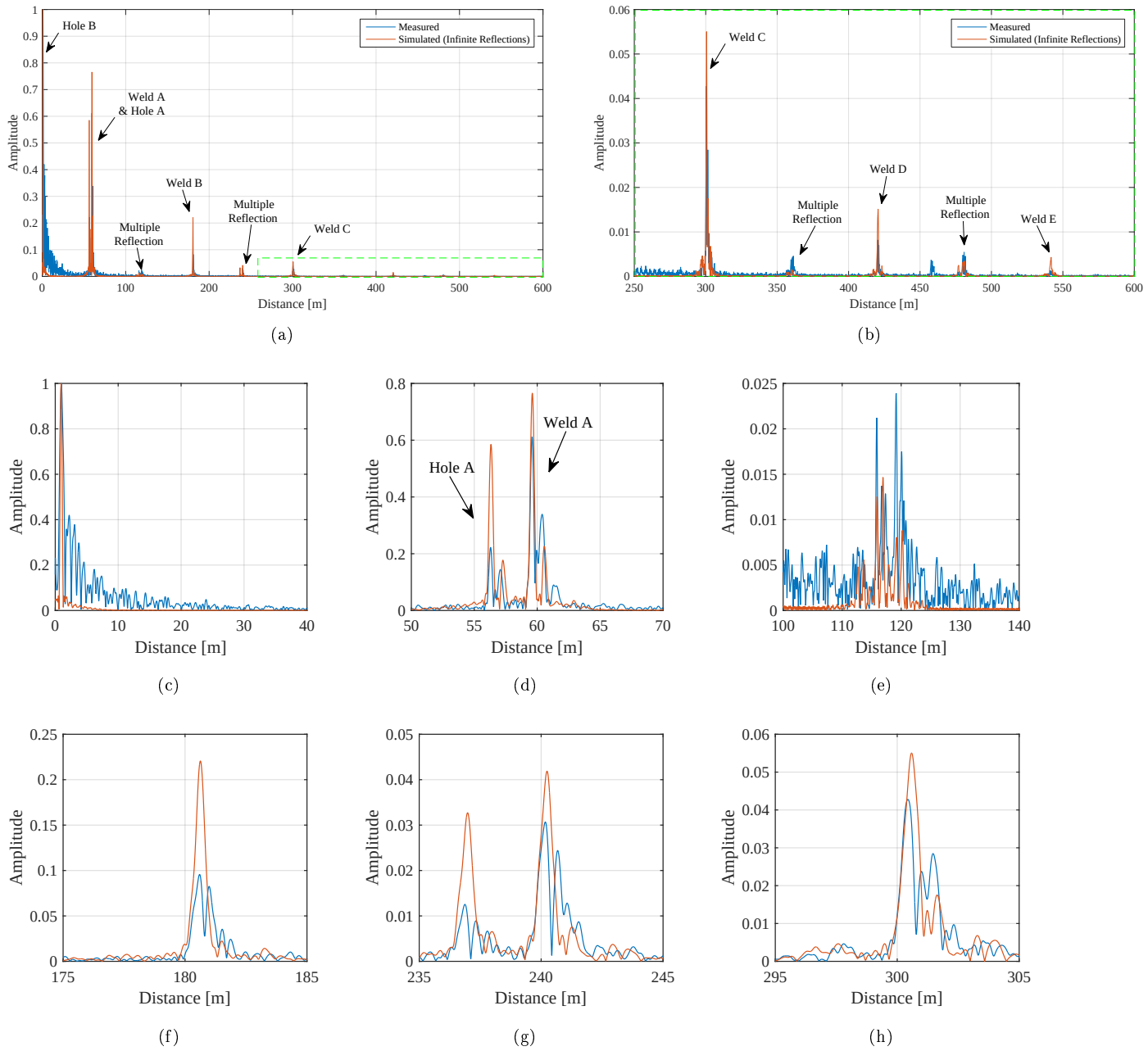


Fig. 11. Distance domain signals of the measured and simulated signals containing infinite reflections. Reflections from (a) welds A to C and the two holes, as well as multiple reflections, (b) welds C to D and other multiple reflections, (c) hole B, (d) weld A and hole A. (e) Multiple reflection. (f) Reflections from weld B. (g) Multiple reflection. (h) Reflections from weld C.

The time domain results presented in Fig. 10 were converted to the distance domain using a dispersion compensation procedure proposed by Wilcox [41]. The dispersion compensation procedure uses the dispersion characteristics of only one mode, and the mode with energy concentrated in the web of the rail (shown in Fig. 7) was used in this case as it is the most prominent. The result in the distance domain is plotted in Fig. 11. It shows the half distance of propagation travelled by each reflection, representing the distance between the transducer and a specific reflector for direct reflections. The distance readings on the horizontal axes in Fig. 11 corresponding to direct reflections, thus gives information about the location of the corresponding reflector from the transducer.

Fig. 11 was studied concurrently with Figs. 6 and 10 to obtain important insights discussed in this section for the inspection at hand. The advantage of the dispersion compensation procedure is clearly visible as the amount of coherent noise in both the field measurement and the simulated signal is minimised.

*4.2. Simulation of finite multiple reflections*

The simulated signal computed using a finite number of reflections, as explained in Section 3, is presented next. Three combinations of reflections were considered to simulate three scenarios. The first signal contained only the eight direct reflections corresponding to each of the eight reflectors. Weld F was included to the left of weld D to have four reflectors on either side of the transducer in the waveguide. Other signals contained 37 and 140 paths, respectively, consisting of both direct and multiple reflections. A schematic representation of propagation paths traced by each reflection for the three scenarios is illustrated in Fig. 12. Scenarios 2 and 3 include more reflections to illustrate the case of complex back and forth reverberations that occur between reflectors due to multiple reflections. Each propagation path represents a unique sequence of reflections and can be traced by following the arrow lines, starting and ending at the transducer location. The horizontal axis in each plot represents the distance axis along the propagation direction of the rail, and the vertical axis represents the propagation time with the times of arrival for each reflection coinciding with the arrowheads located at the transducer location, at distance $z = 0$. The schematic representation of propagation paths was constructed by tracking the amplitude and propagation distances and times of arrival for each unique reflection during the computation process using the procedure in Section 3 and reference [34]. The reflections included in each case were selected based on the distance of propagation and the energy of the waves.

Fig. 13 lists some of the reflections from the simulation, with each entry describing the propagation path traced by a reflection and the associated distance of propagation divided by two. The figure shows direct and multiple reflections for the first 24 reflections and selected direct reflections from long-range distances. The multiple reflections are classified according to the number of times the propagating energy would reflect off discontinuities.

The resultant time domain signals for the three cases in Fig. 12 were constructed. The residual between each simulated signal and the signal simulated with infinite reflections is computed and compared in Fig. 14. The results show that when only the eight direct reflections are included in the simulation, many reflections are not captured in the simulated signal. The absent reflections correspond to multiple reflections as they were not included for that case. The simulation with 37 reflections shows an improvement in the number of reflections captured. The simulation containing 140 reflections further improves captured reflections, especially those that arrive late. The result for 140 reflections still shows a lot of residual for reflections arriving very early. First, the field measurement contains noticeable coherent noise in this region and second, multiple reflections due to sleepers in the rail were not included in the simulation.

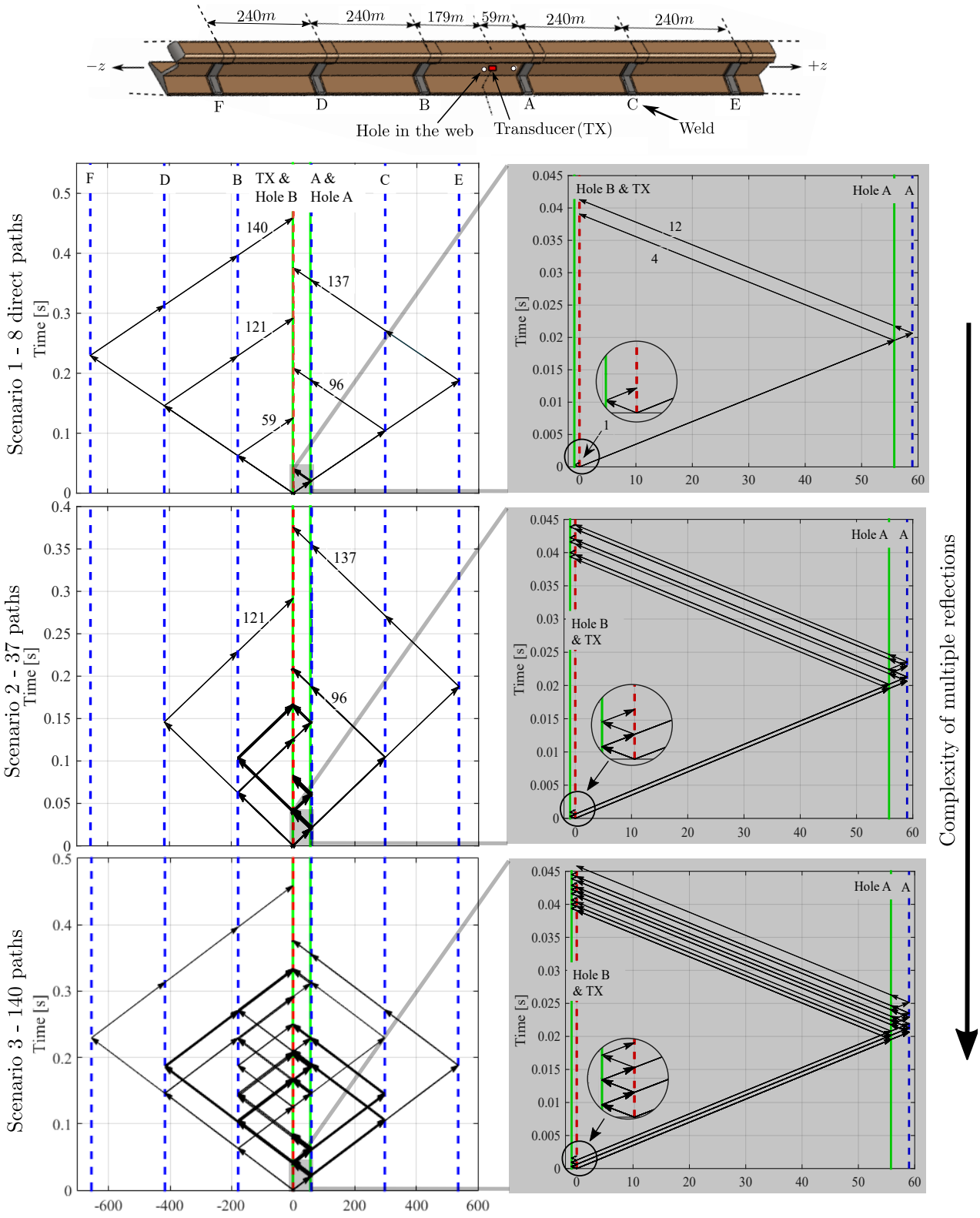


Fig. 12. Schematic representation of direct and multiple propagation paths labelled according to Fig. 13. Eight direct paths in scenario 1, 37 paths (direct and multiple) in scenario 2, and 140 paths (direct and multiple) for scenario 3. Details of complex reflection paths from the 3 scenarios are highlighted on the plots on the right, zooming around selected paths.

| Path # | Distance [m] | Path Description |
|---|---|---|
| 1 | 0.91 | TX HB TX |
| 2 | 1.82 | TX HB TX HB TX |
| 3 | 2.73 | TX HB TX HB TX HB TX |
| 4 | 55.78 | TX HA TX |
| 5 | 56.70 | TX HB TX HA TX |
| 6 | 56.70 | TX HA TX HB TX |
| 7 | 57.61 | TX HB TX HB TX HA TX |
| 8 | 57.61 | TX HB TX HA TX HB TX |
| 9 | 57.61 | TX HA TX HB TX HB TX |
| 10 | 58.52 | TX HB TX HB TX HA TX HB TX |
| 11 | 58.52 | TX HB TX HA TX HB TX HB TX |
| 12 | 58.99 | TX HA WA HA TX |
| 13 | 59.90 | TX HB TX HA WA HA TX |
| 14 | 59.90 | TX HA WA HA TX HB TX |
| 15 | 60.81 | TX HB TX HB TX HA WA HA TX |
| 16 | 60.81 | TX HB TX HA WA HA TX HB TX |
| 17 | 60.81 | TX HA WA HA TX HB TX HB TX |
| 18 | 61.72 | TX HB TX HB TX HA WA HA TX HB TX |
| 19 | 61.72 | TX HB TX HA WA HA TX HB TX HB TX |
| 20 | 62.20 | TX HA WA HA WA HA TX |
| 21 | 63.11 | TX HB TX HA WA HA WA HA TX |
| 22 | 63.11 | TX HA WA HA WA HA TX HB TX |
| 23 | 64.02 | TX HB TX HA WA HA WA HA TX HB TX |
| 24 | 65.41 | TX HA WA HA WA HA WA HA TX |
| 59 | 178.89 | TX HB WB HB TX |
| 96 | 297.69 | TX HA WA WC WA HA TX |
| 121 | 416.57 | TX HB WB WD WB HB TX |
| 137 | 536.39 | TX HA WA WC WE WC WA HA TX |
| 140 | 655.63 | TX HB WB WD WF WD WB HB TX |

**Key**

- Direct Reflections
- Double Reflections
- Tripple Reflections
- Higher Order Reflections

| | |
|---|---|
| TX | Transducer |
| Hi | Hole i |
| Wi | Weld i |

Fig. 13. Description of propagation paths for selected reflections.

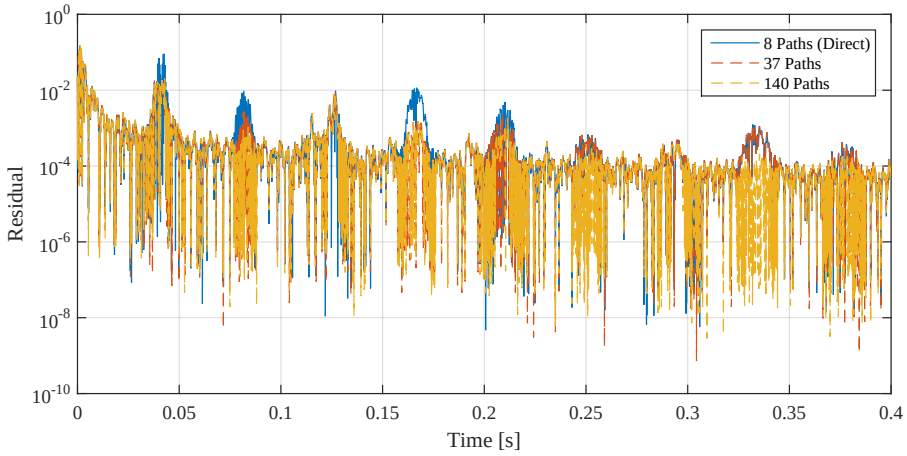


Fig. 14. Residual signals between the simulation with infinite and finite reflections.

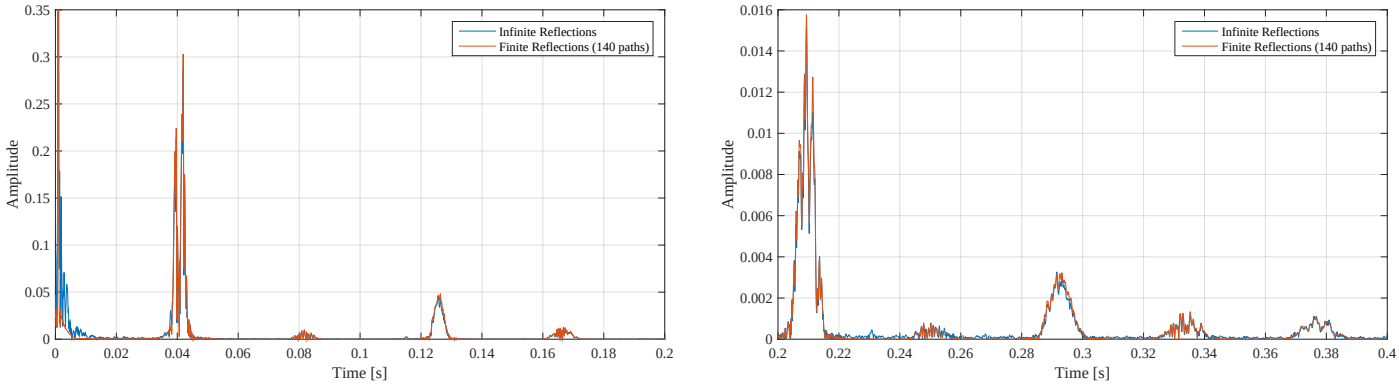


Fig. 15. Comparison of simulated signals. (a) Time window from 0s to 0.2s. (b) Time window from 0.2s to 0.4s.

Fig. 15 shows a comparison plot between the simulated signals constructed from infinite reflections and 140 finite reflections, respectively. The comparison shows that the simulation with 140 reflections is acceptable though some features were not captured. A further improvement could be achieved by including more reflections in the simulation. However, this would result in a tedious process with little improvement.

In the next section, the simulated signal containing 140 reflections is interpreted using decomposition of reflections to analyse the measurement at hand for a better understanding of the behaviour of reverberating reflections.

### *4.3. Analysis and interpretation of the GWU inspection*

Plots of the time domain and distance domain signals simulated using 140 reflections are shown in Figs. 16 and 17, respectively. The resultant signal constructed by adding individual reflection paths is plotted using the thick solid blue curve, and the other curves represent each of the 140 reflections. The legend for these plots is shown in Appendix A in Fig. A.1.

The first characteristic noticed in the simulated data is the effect introduced by dispersion and the significant role of the dispersion compensation procedure of Wilcox [41]. The superposition of individual reflections and the resultant signal in the time domain represents dispersion effects. This is highlighted by the complexity of the signals in Fig. 16 and the severe overlapping of reflections. However, the signals become less complex with reduced overlapping of reflections once the dispersion effects are compensated for, Fig. 17. This behaviour is most obvious when comparing, for example, the corresponding pair of sub-figures in Figs. 16 and 17. Another behaviour worth noting while comparing the pair of figures is the distortions in the burst of energies. The explicit cause for this is, of course, the overlapping of reflections, but dispersion seems to be the primary cause as there is less distortion in the distance domain signals.

Second, we notice that there is almost no overlapping for some direct reflections, for example, those associated with weld A and hole A in Figs. 16a and 17a, weld B in Figs. 16c and 17c, and weld C in Figs. 16e and 17e. In contrast, weld D in Figs. 16g and 17g and weld E in Figs. 16i and 17i show that some reflections overlap with these direct reflections. However, there exist pairs of overlapping reflections just after the direct reflection for hole A and welds A and C, respectively, Figs. 17a&e. These reflections are believed to be visible multiple reflections that occur within this region.

Thirdly, prominent multiple reflections also seem to be overlapping in pairs, for example, multiple reflections 2, 3 and 4. Let us look at the resultant signal and the overlapping reflections. We notice two pairs of overlapping multiple reflections in Fig. 17d, almost four pairs of overlapping multiple reflections in Fig. 17f and three pairs of overlapping multiple reflections in Fig. 17h.

Lastly, we further notice the high complexity of multiple reflections, which is evident in the sub-figure labelled as multiple reflections 1 in Fig. 17b. Here, there are many multiple reflections, with the resultant of

some reflections made by an overlap of more than two reflections. The reflections contributing to the resultant signal in Figs. 16a and 17a corresponds to entries 4 to 20 in Fig. 13. The two multiple reflections in the resultant signal with a pair of overlapping reflections as identified in those figures earlier on are constructed from reflection paths 5 & 6 and reflection paths 13 & 14, respectively. The multiple reflections propagating a distance of 56.70m×2 are double reflections happening between holes A and B.

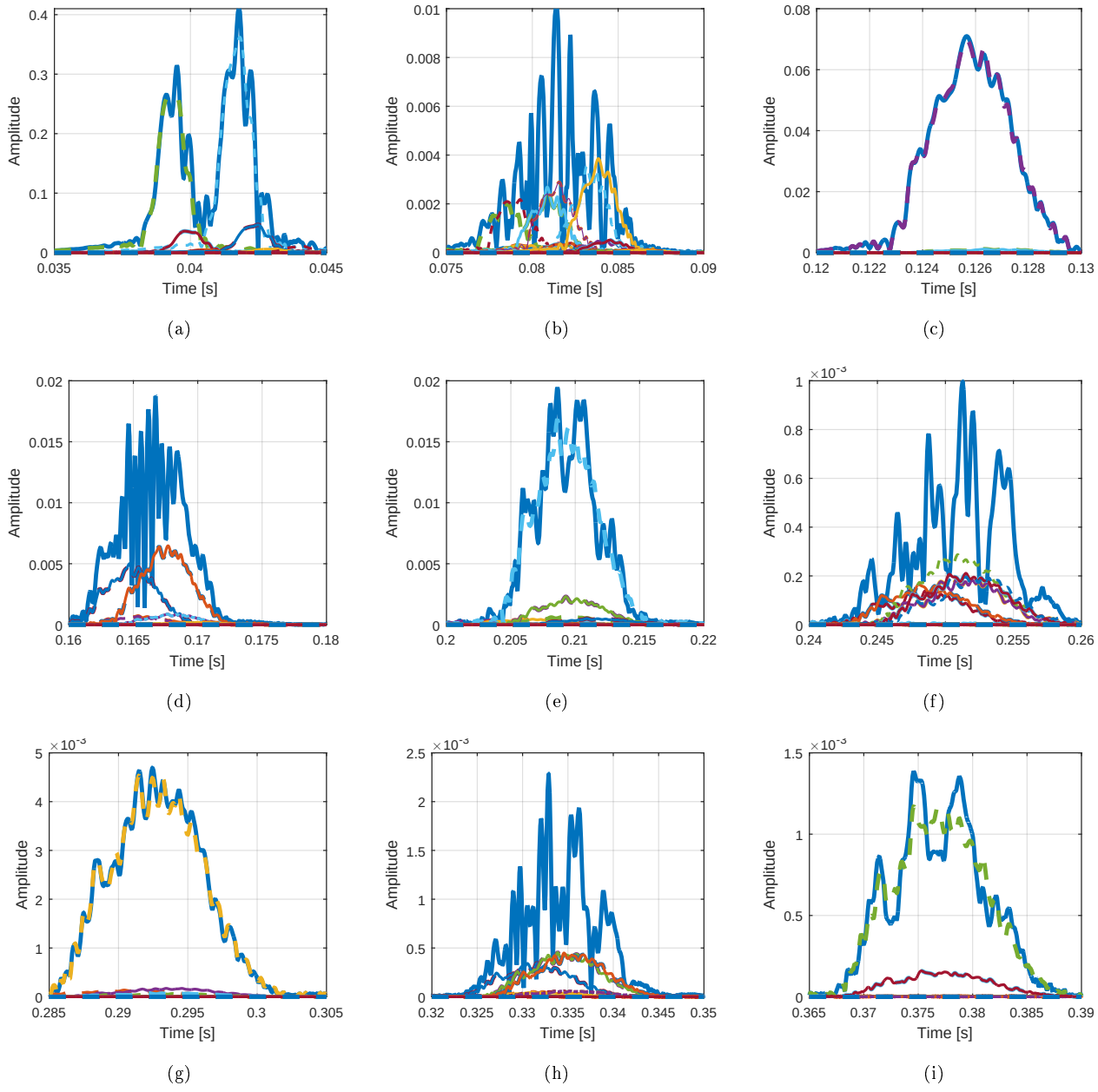


Fig. 16. Time history of the simulated signal containing 140 infinite reflections. (a) Reflections from weld A and hole A. (b) Multiple reflection 1. (c) Reflection from weld B. (d) Multiple reflection 2. (e) Reflection from weld C. (f) Multiple reflection 3. (g) Reflections from weld D. (h) Multiple reflection 4. (i) Reflections from weld E.

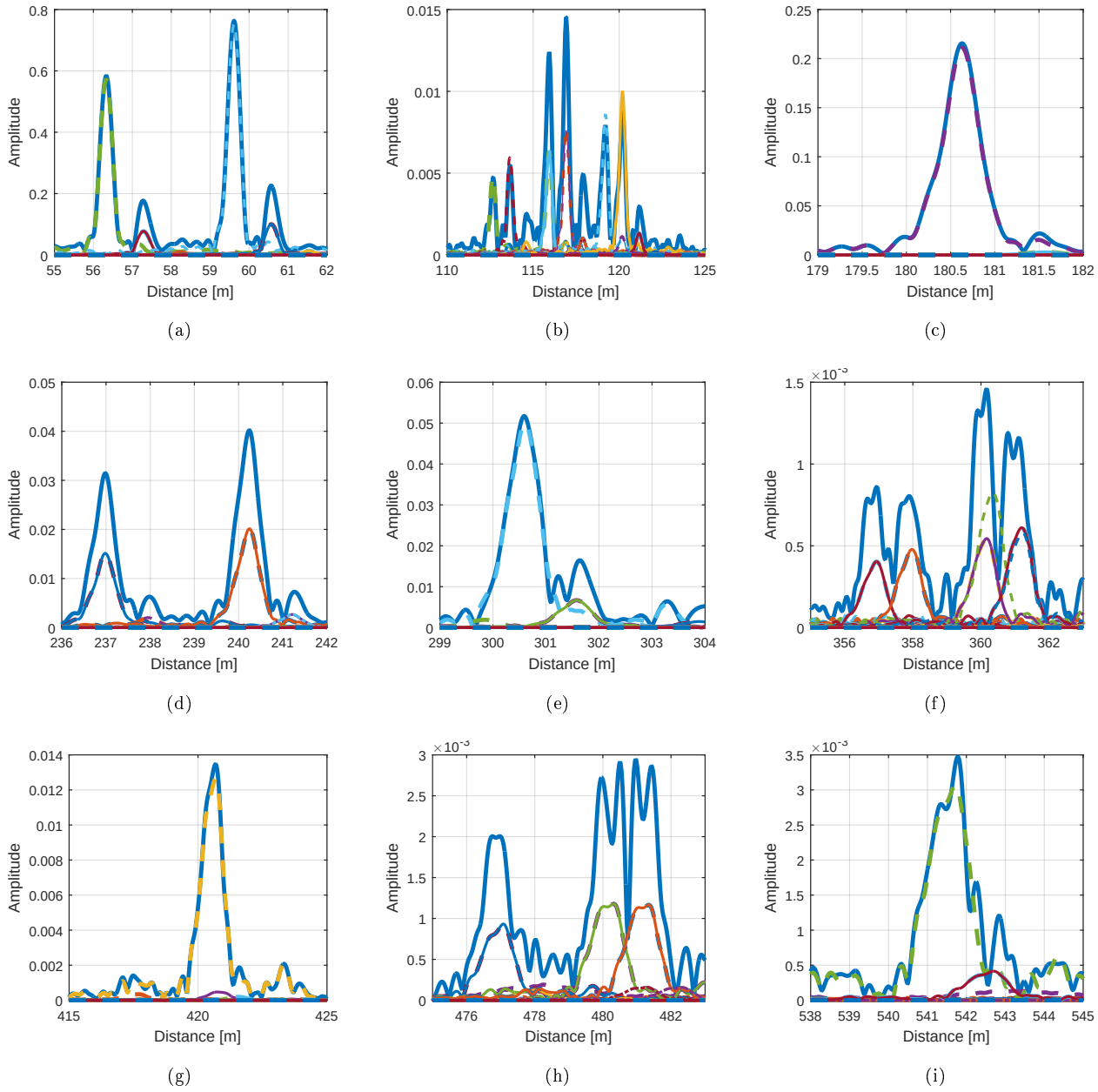


Fig. 17. Distance domain signal of the simulated signal containing 140 reflection paths. (a) Reflections from weld A and hole A. (b) Multiple reflection 1. (c) Reflection from weld B. (d) Multiple reflection 2. (e) Reflection from weld C. (f) Multiple reflection 3. (g) Reflections from weld D. (h) Multiple reflection 4. (i) Reflections from weld E.

## 5. Conclusion

Two numerical procedures to model and simulate complete guided wave inspections encompassing the excitation, propagation and scattering from discontinuities located on either side of the transducer in 1D waveguides were presented. The major contribution highlighted by these procedures is the ability to simulate the complex back and forth reverberating reflections that occur between structural features such as welds and other discontinuities such as damage. The two approaches are different but complementary. The first one is based on simple manual simulation of finite reverberating reflections and offers the ability to perform a thorough analysis of the resultant simulation to better understand how different reflections interact with each other, especially where

they overlap. The second method is based on a general scattering matrix computation. It offers a more accurate approximation of the simulated inspection since it accounts for infinite reverberations.

The results simulated with the two modelling procedures were validated using a field experiment from a damage-free rail containing welds and holes as discontinuities. The most notable characteristics, namely the arrival times of the dominant reflections and attenuation, were accurately captured in the simulated result. The time domain signals were far more complex due to high coherent noise and effects of dispersion. The simulation procedure using finite reflections illustrated the advantage of the dispersion compensation procedure as the amount of complexity was reduced, which helped with the interpretation of reflections. This demonstrated the benefit of studying different representations of results concurrently to obtain better insights. Multiple reflections were more complex than direct reflections, with many overlapping and occurring around the same region. Though there was almost no overlapping for direct reflections, some multiple reflections were occurring very close to them, showing the significance of accounting for multiple reflections in simulated inspections. While the simulation procedure helped identify the sources of reflections and understand complex back and forth propagation paths traced by these reflections, it also made it possible to spot reflections that were not apparent in the field measurement due to noise masking those reflections. The procedure in Section 3.2 gave a good approximation of the simulated inspection, while the procedure in Section 3 allowed for interpretation of results which helped with the understanding of the reverberations in the response signals.

In conclusion, this study illustrated that a reliable numerical model could be useful when interpreting experimental results since it can simulate features that are not apparent in the experiment. In future, the modelling approaches will be adopted to simulate and study inspections for unavailable damage scenarios and also to benefit digital twin models.

## Appendix A

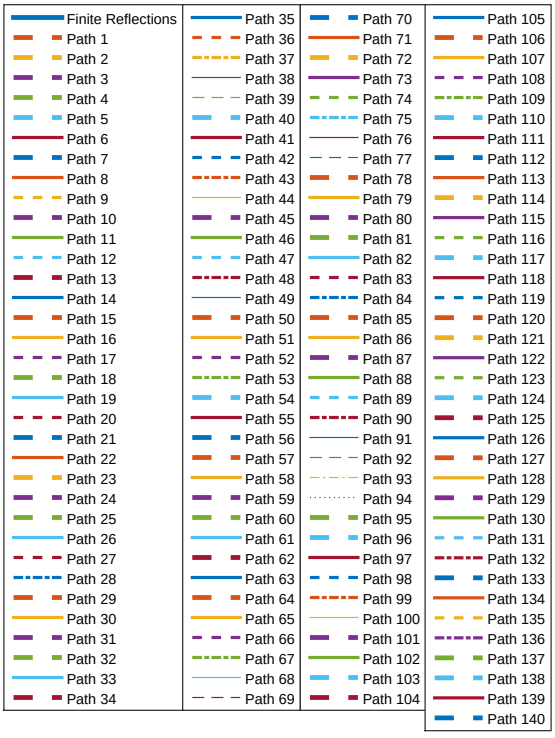


Fig. A.1. A legend for Figs. 16 and 17.

## References


[1] P. Cawley, F. Cegla, A. Galvagni, Guided waves for NDT and permanently-installed monitoring, Insight: Non-Destructive Testing and Condition Monitoring 54 (11) (2012) 594–601. doi:10.1784/insi.2012.54.11.594.

[2] P. Cawley, Structural health monitoring: Closing the gap between research and industrial deployment, Structural Health Monitoring 17 (5) (2018) 1225–1244. doi:10.1177/1475921717750047.

[3] P. Loveday, D. Ramatlo, F. Burger, Monitoring of rail track using guided wave ultrasound, in: Proceedings of the 19th World Conference on Non Destructive Testing (WCNDT 2016), 2016, pp. 3341–3348.

[4] F. Burger, P. Loveday, Ultrasonic broken rail detector and rail condition monitor technology, in: Proceedings of the 11th International Heavy Haul Association Conference (IHHA 2017), no. September, 2017, pp. 275–280.

[5] P. Loveday, C. Long, D. Ramatlo, Ultrasonic guided wave monitoring of an operational rail track, Structural Health Monitoring 19 (6) (2020). doi:10.1177/1475921719893887.

[6] C. Liu, J. Dobson, P. Cawley, Practical Ultrasonic Damage Monitoring on Pipelines Using Component Analysis Methods, in: 19th World Conference on Non-Destructive Testing 2016, 2016, pp. 1–8.

[7] J. Dobson, P. Cawley, Independent component analysis for improved defect detection in guided wave monitoring, Proceedings of the IEEE 104 (8) (2016) 1620–1631. doi:10.1109/JPROC.2015.2451218.

[8] C. Liu, J. Dobson, P. Cawley, Efficient generation of receiver operating characteristics for the evaluation of damage detection in practical structural health monitoring applications, Proceedings of the Royal Society A: Mathematical, Physical and Engineering Sciences 473 (2199) (2017) 1–26. doi:10.1098/rspa.2016.0736.

[9] H. Sohn, Effects of environmental and operational variability on structural health monitoring, Philosophical Transactions of the Royal Society A: Mathematical, Physical and Engineering Sciences 365 (1851) (2007) 539–560. doi:10.1098/rsta.2006.1935.

[10] T. Clarke, F. Simonetti, P. Cawley, Guided wave health monitoring of complex structures by sparse array systems: Influence of temperature changes on performance, Journal of Sound and Vibration 329 (12) (2010) 2306–2322. doi:10.1016/j.jsv.2009.01.052.

[11] A. J. Croxford, J. Moll, P. D. Wilcox, J. E. Michaels, Efficient temperature compensation strategies for guided wave structural health monitoring, Ultrasonics 50 (4-5) (2010) 517–528. doi:10.1016/j.ultras.2009.11.002.

[12] J. B. Harley, J. M. Moura, Scale transform signal processing for optimal ultrasonic temperature compensation, IEEE Transactions on Ultrasonics, Ferroelectrics, and Frequency Control 59 (10) (2012) 2226–2236. doi:10.1109/TUFFC.2012.2448.

[13] S. Mariani, S. Heinlein, P. Cawley, Compensation for temperature-dependent phase and velocity of guided wave signals in baseline subtraction for structural health monitoring, Structural Health Monitoring 19 (1) (2020) 26–47. doi:10.1177/1475921719835155.

[14] S. Mariani, S. Heinlein, P. Cawley, Location specific temperature compensation of guided wave signals in structural health monitoring, IEEE Transactions on Ultrasonics, Ferroelectrics, and Frequency Control 67 (1) (2020) 146–157. doi:10.1109/TUFFC.2019.2940451.

[15] I. I. Setshedi, P. W. Loveday, C. S. Long, D. N. Wilke, Estimation of rail properties using semi-analytical finite element models and guided wave ultrasound measurements, Ultrasonics 96 (July 2018) (2019) 240–252. doi:10.1016/j.ultras.2018.12.015.

[16] I. Bartoli, F. Lanza Di Scalea, M. Fateh, E. Viola, Modeling guided wave propagation with application to the long-range defect detection in railroad tracks, NDT and E International 38 (5) (2005) 325–334. doi:10.1016/j.ndteint.2004.10.008.

[17] C. A. Leckey, K. R. Wheeler, V. N. Hafiychuk, H. Hafiychuk, D. A. Timuçin, Simulation of guided-wave ultrasound propagation in composite laminates: Benchmark comparisons of numerical codes and experiment, Ultrasonics 84 (2018) 187–200. doi:10.1016/j.ultras.2017.11.002.

[18] M. M. Narayanan, A. Kumar, S. Thirunavukkarasu, C. K. Mukhopadhyay, Development of ultrasonic guided wave inspection methodology for steam generator tubes of prototype fast breeder reactor, Ultrasonics 93 (October 2018) (2019) 112–121. doi:10.1016/j.ultras.2018.11.003.

[19] C. S. Long, P. W. Loveday, D. A. Ramatlo, E. V. Andhavarapu, Numerical verification of an efficient coupled SAFE-3D FE analysis for guided wave ultrasound excitation, Finite Elements in Analysis and Design 149 (2018) 45–56. doi:10.1016/j.finel.2018.05.001.
URL https://doi.org/10.1016/j.finel.2018.05.001

[20] L. Gavric, Computation of propagative waves, Journal of Sound and Vibration 185 (3) (1995) 531–543.

[21] T. Hayashi, W. J. Song, J. L. Rose, Guided wave dispersion curves for a bar with an arbitrary cross-section, a rod and rail example, Ultrasonics 41 (3) (2003) 175–183. doi:10.1016/S0041-624X(03)00097-0.
URL http://linkinghub.elsevier.com/retrieve/pii/S0041624X03000970

[22] I. Bartoli, A. Marzani, F. Lanza di Scalea, E. Viola, Modeling wave propagation in damped waveguides of arbitrary cross-section, Journal of Sound and Vibration 295 (3-5) (2006) 685–707. doi:10.1016/j.jsv.2006.01.021.

[23] E. Leinov, M. J. Lowe, P. Cawley, Investigation of guided wave propagation and attenuation in pipe buried in sand, Journal of Sound and Vibration 347 (2015) 96–114. doi:10.1016/j.jsv.2015.02.036.
URL http://dx.doi.org/10.1016/j.jsv.2015.02.036

[24] F. Benmeddour, F. Treyssède, L. Laguerre, Numerical modeling of guided wave interaction with non-axisymmetric cracks in elastic cylinders, International Journal of Solids and Structures 48 (5) (2011) 764–774. doi:10.1016/j.ijsolstr.2010.11.013.
URL http://dx.doi.org/10.1016/j.ijsolstr.2010.11.013

[25] C. S. Long, P. W. Loveday, Analysis of guided wave scattering due to defects in rails using a hybrid FE-safe method, in: AIP Conference Proceedings, Vol. 1511, 2013, pp. 238–245. doi:10.1063/1.4789054.
URL http://link.aip.org/link/APCPCS/v1511/i1/p238/s1&Agg=doi

[26] C. S. Long, P. W. Loveday, Prediction of guided wave scattering by defects in rails using numerical modelling, in: AIP Conference Proceedings, Vol. 1581 33, 2014, pp. 240–247. doi:10.1063/1.4864826.

[27] P. W. Loveday, Analysis of piezoelectric ultrasonic transducers attached to waveguides using waveguide finite elements, IEEE Transactions on Ultrasonics, Ferroelectrics, and Frequency Control 54 (10) (2007) 2045–2051. doi:10.1109/TUFFC.2007.499.

[28] D. A. Ramatlo, D. N. Wilke, P. W. Loveday, Development of an optimal piezoelectric transducer to excite guided waves in a rail web, NDT and E International 95 (2018) 72–81. doi:https://doi.org/10.1016/j.ndteint.2018.02.002.

[29] K. Jezzine, A. Lhemery, Reciprocity Principle and the Semi-Analytical Finite, Physics 26 39–46.

[30] V. BARONIAN, K. JEZZINE, S. CHATILLON, Numerical methods for scattering by inhomogeneities in 3D elastic waveguides (Ecndt) (2014).

[31] V. Baronian, K. Jezzine, Simulation of NDT Inspection in 3D Elastic Waveguide Involving Arbitrary Defect, 19th World Conference on Non-Destructive Testing 2016 Simulation (2016) 1–8.
URL http://www.wcndt2016.com/Programme/show/We-4-H-3

[32] Ultrasonic testing with civa, accessed: 2020-04-03.
URL www.extende.com

[33] V. Baronian, A. Lhémery, K. Jezzine, Hybrid SAFE/FE simulation of inspections of elastic waveguides containing several local discontinuities or defects, AIP Conference Proceedings 1335 (June) (2011) 183–190. doi:10.1063/1.3591855.

[34] D. A. Ramatlo, C. S. Long, P. W. Loveday, D. N. Wilke, A modelling framework for simulation of ultrasonic guided wave-based inspection of welded rail tracks, Ultrasonics 108 (September 2019) (2020) 106215. doi:10.1016/j.ultras.2020.106215.
URL https://doi.org/10.1016/j.ultras.2020.106215

[35] L. Margerin, G. Nolet, Multiple scattering of high-frequency seismic waves in the deep Earth: Modeling and numerical examples, Journal of Geophysical Research: Solid Earth 108 (B5) (2003). doi:10.1029/2002jb001974.

[36] F. Sagnard, G. El Zein, In situ characterization of building materials for popagation modeling: Frequency and time responses, IEEE Transactions on Antennas and Propagation 53 (10) (2005) 3166–3173. doi:10.1109/TAP.2005.856333.

[37] J. B. Harley, M. U. Saleh, S. Kingston, M. A. Scarpulla, C. M. Furse, Fast transient simulations for multi-segment transmission lines with a graphical model, Progress in Electromagnetics Research 165 (January) (2019) 67–82. doi:10.2528/pier19042105.

[38] D. Smagulova, L. Mazeika, E. Jasiuniene, Novel processing algorithm to improve detectability of disbonds in adhesive dissimilar material joints, Sensors 21 (9) (2021). doi:10.3390/s21093048.

[39] S. K. Pedram, T. H. Gan, M. Ghafourian, Improved defect detection of guided wave testing using split-spectrum processing, Sensors (Switzerland) 20 (17) (2020) 1–18. doi:10.3390/s20174759.

[40] P. W. Loveday, Simulation of piezoelectric excitation of guided waves using waveguide finite elements, IEEE Transactions on Ultrasonics, Ferroelectrics, and Frequency Control 55 (9) (2008) 2038–2045.

[41] P. D. Wilcox, A Rapid Signal Processing Technique to Remove the Effect of Dispersion from Guided Wave Signals, IEEE Transactions on Ultrasonics, Ferroelectrics, and Frequency Control 50 (4) (2003) 419–427.